Evaluation of Performance of Resistance Spot Welded Joints with Different Parameters in Advanced High Strength TRIP Steel

I. Hajiannia[1,*], R. Ashiri[2], M. R. Pakmanesh[3], M. Shamanian[1], M. Atapour[1]

[1] *Department of Materials Engineering, Isfahan University of Technology, Isfahan, Iran.*
[2] *Department of Materials Science and Engineering, Dezful Branch, Islamic Azad University, Dezful, Iran.*
[3] *Iran Institutes of Materials and Energy, Iranian Space Research Center, Isfahan, Iran.*
Received: 21 *August 2018 – Accepted: 27 December 2018*

Abstract

In this research, ultrahigh strength transformation induced plasticity-assisted steel (TRIP-assisted steel) was developed to be used in the automobile body. For this, it is essential to characterize its weldability in resistance spot welding process. Therefore, the resistance spot welding metallurgy and weldability of the steel under different welding parameters are studied. the desired sample was studied in two states with higher pressure and less time. The results are presented following the most important advantage of the current steel in contrast to the similar steels is its excellent weldability enabling its application in the auto pillar. The microstructure and mechanical properties of TRIP steel spot welds were characterized using metallurgical techniques, lap shear tensile tests fractography and microhardness testing methods. Failure mode transition from interfacial to pullout failure mode was achieved for sample 10kA with 4kN. Partial interfacial failure was removed after nugget size increased. Pullout failure mode is seen for the sample 2, 10kA with 3.5kN.

Keywords: TRIP Steel, Resistance Spot Welding, Mechanical Properties, Failure Mode.

1. Introduction

Transformation-induced plasticity (TRIP) steel is an advanced high strength steel (AHSS). The popularity of advanced high strength steels (AHSSs) is increasing recently because of their strength and ductility synergy. They have been applied widely in the automotive industries to decrease weight simultaneous with improvement in vehicle safety [1-3]. Usually, the microstructure of the steel consists of bainite, martensite, and retained austenite in a matrix of the soft ferrite [4,5]. Resistance spot welding (RSW) is a reliable welding method wherein molten zone is formed between steel sheets [6]. Meanwhile, the resistance spot welding (RSW) is the most widely used method to join sheet metals in the automotive industry.

These steels are known as TRIP steels because the retained austenite transforms to martensite at high strains resulting in an excellent work hardenability persisting over a large amount of strain [7, 8]. However, the weldability of these steels has been an ongoing concern due to the high amounts of carbon and other austenite stabilizers, which can produce hard microstructures in the weld zone since high cooling rates are experienced in RSW. When performing RSW, microstructural changes in the fusion zone (FZ) and surrounding heat affected zone (HAZ) affect the weld mechanical properties which need to be specified to develop optimized welding procedures for these steels [9, 10].

*Corresponding author
Email address: i.hajiannia@ma.iut.ac.ir

Gaul et al. [11] studied methods to obtain weld discontinuities in the spot-welded joints made of AHSSs. They showed that RSW of AHSSs in clump manufacture lead to weld discontinuities under some specific conditions. Two main causes noted in this study for weld discontinuities are the welding parameters and the special production. Weber et al. [12] conducted a study on the weldability and welding parameter effects in RSW of AHSSs. The results showed that the welding time has considerable effects on quality and tensile-shear strength of the welds, but the electrode force is insignificant. Load bearing capacity in AHSSs is higher than that of the tested mild steel. Pakkanen et al. [13] studied RSW of advanced high strength dual phase steel with a tensile strength of 980 MPa and a fracture elongation of 10 %. Moreover, the effects of welding current on nugget size and residual stresses were examined for low, medium and high welding currents inside weldable current range. The results showed the simulations did not comply with experimental residual stress obtained from drill hole technique and the measured nugget size. High strength steels have shown moderate weldability compared to mild steels. If common resistance spot welding parameters are used for these steels, partial plug failure and interfacial failure modes are likely to occur. It has been proven that the interfacial failure is weighed to be brittle with minimum energy absorption in contrast to the plug failure [14]. Because of the above conditions, the welding parameters should be set in the best conditions to achieve the best mechanical properties. In summary, study the resistance spot welding metallurgy of the

Table. 1. Chemical composition of the experimental TRIP steel (wt. %)

C	Si	Mn	S	P	Al	Cr	Ni	Fe
0.180	1.030	2.450	0.009	0.003	0.010	0.020	0.030	Bal.

Table. 2. Carbon equivalent and calculated critical temperatures for the alloy [10].

Melting point (°C)	A_{C3} (°C)	A_{C1} (°C)	C_{eq}
1545	858	720	0.62%

newly developed TRIP steel at different welding conditions is the main aim of the research.
Mechanical properties and failure mode were studied and reported in previous studies [2,3 , 8,9] but weldability and mechanical properties of the high strength TRIP steels with rich chemical composition have not been evaluated yet.
Therefore, it is necessary to conduct research on the current steel to obtain the optimal conditions in the resistance spot welding to assess the possibility of its application in the autobody.
To better understand the metallurgical phenomena, microstructure and mechanical properties of the welds the resistance spot welding of the newly developed TRIP steel is studied in-depth.

2. Materials and Methods

New ultrahigh strength TRIP-assisted steel was formed under special thermomechanical conditions with the following processing details. The ingots with dimensions of 100mm×100mm×50 mm were casted using an electric furnace, and then were homogenized at 1000°C for 1 hr.
Afterwards, hot rolling was used to reduce the thickness of the ingots down to 3.2 mm, and then they were pickled in HCl, and finally the thickness was cold rolled down to 1 mm. Table. 1. given the chemical composition of the above mentioned steel sheets.
A two-stage heat treatment was done on the alloy to obtain bainite with austempering heat treatment. First, the cold rolled sheet was heat treated in two steps using two salt baths to achieve a typical microstructure of TRIP steel. Strips were intercritically annealed at 780 °C for 300s, and then were immediately moved to another salt furnace bath with temperature of 350°C and held there for 600s for the progress in the bainitic transformation [15].
The heat treatment is shown in Fig. 1., schematically. In the second stage, they were heat treated at 350°C for 600s, and then were quenched in water rapidly. Ac1 and Ac3 temperatures for the alloy were calculated to be 720°C and 858 °C, respectively. In welding, carbon equivalent content (CE) is used to show the contributions of the different alloying elements in the hardness of the steel being welded.

This is then directly related to hydrogen induced cold cracking, which is the most common weld defect for the steel [5], thus it is the most commonly used factor to determine the weldability of the alloy.

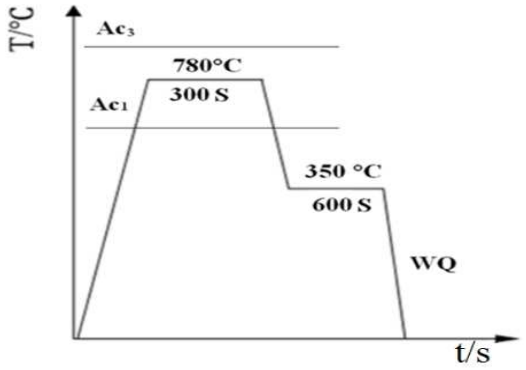

Fig. 1. Schematic diagram of heat treatment process, used for obtaining the retained austenite in the steel.

According to the carbon equivalent (CE) formula (Eq. 1) [10] CE of the alloy was calculated and given in Table. 2.

$$CE=\%C+\%Mn/6+(\%Cr+\%V)/5+\%Si/15 \quad \text{Eq. (1)}$$

X-ray diffraction (XRD) in a Philips MPD diffractometer using filtered Cu Ka radiation (k = 0.15406 nm).was used to determine the volume fraction of the retained austenite (RA) according to the ASTM E975 standard [19]. RA was calculated by the integrated intensities of ferrite and austenite phases from XRD patterns. PANalytical X'pert High Score Plus software was used to analyze integral intensities and 2θ angles, carbon concentration (wt. %) in austenite and the lattice constants. The equation 2 was used to determine the volume fraction of RA (VA) Eq. (2) [6]:

$$V_{A=} 1.4I_{A/} 1.4I_A+I_F \quad \text{Eq. (2)}$$

Where IA and IF are the integrated intensities of the $(200)_A$, $(220)_A$, $(311)_A$ peaks, $(200)_F$ and $(211)_F$ peaks, respectively.
VA has been calculated as 15% for the current TRIP steel.

Table. 3. Mechanical properties of the steel studied [7].

Specimen	Yield Strength (MPa)	Tensile Strength (MPa)	Total Elongation (%)
Ultrahigh Strength TRIP Steel	616 ± 20	1114 ± 20	25 ± 1

Tablel. 4. Resistance spot welds mechanical responses in tensile shear test.

Weld Parameters					Tensile Shear Strength	
Sample	**Current (kA)**	**Force (kN)**	**Nugget Size (mm)**	**Hold Time Cycles**	**Maximum Load (kN)**	**Failure Mode**
1	10	3.5	5.15	5	4.9	Interfacial fracture with partial thickness fracture
2	10	3.5	5.7	10	6.85	button pullout and partial thickness fracture
3	10	4	5.45	10	10.5	Interfacial fracture with button pullout and partial thickness fracture

2.1. Mechanical Properties Evaluation

The tensile tests were performed by Instron universal testing machine, Instron 3300. Samples were prepared in accordance with ASTM A370 standard [5]. The thickness of the specimens was 1 mm and their gage length was 50 mm all tests were performed at room temperature and the crosshead velocity was maintained at a constant rate of 1 mm min^{-1}. Engineering strength of the base metal was obtained in Table. 3., respectively. All the welded samples were exposed to a tensile-shear test to determine the joint strength. The lap shear tensile test was used to characterize the mechanical properties of the welds. Samples were prepared following ANSI/AWS/SAE/D8.9-97 standards [9]. All tests were performed at room temperature. At least two samples were tested for repeatability tests. The crosshead velocity was maintained at a constant rate of 1 mm min^{-1}.

2.2. Metallographic Evaluation

Metallographic cross-sectioned samples were prepared and optical Nikon Model S microscopy (OM) and SEM observations were carried out by a Philips XL30 scanning electron microscope operating at 20 kV. techniques were used to examine the weld microstructures.
Specimens for microstructural analysis were mounted, ground and polished to 2400 grit finish and then polished with 0.3 µm alumina suspension. They were later etched for 5s using 2% nital for study the microstructure [3].

2.3. Materials and Welding Processes

Test samples were welded by a pneumatic, phase-shift controlled DC spot welding machine with 60 kVA capacity in 50 Hz electrical circuit.
Electrode used in RSW was a truncated RWMA class 2 type with 6 mm face diameter.
A constant flow of water (4 L/min) was maintained to cool the electrodes.
The welding conditions are given in Table. 4.
Presented steel are classified according to minimum ultimate tensile strength in group four, AWS D8.1M:2013 [5].

3. Results and Discussion

3.1. Microstructural Evaluation

The microstructure of the received TRIP steel contains bainite, martensite, and retained austenite phases embedded in a ferrite matrix [16], as seen in Fig. 2. SEM micrographs,
As is observed in Fig. 2., the fine grains of 1µm size were obtained through simultaneous tailoring of the heat treatment and cold rolling processes.
The blocky RA forms within the M/A island whereas the RA between the bainite laths appears in the form of very fine grains.
The size of polygonal ferrite grains is between 0.5 and 4 µm and that of M/A island phase is between 1 and 2 µm.
Using the load displacement diagram, two variables of 1(the maximum load) and 2 fracture energy up to maximum load were determined.
Fracture energy, as the area under the load-displacement diagram to the maximum load point, was calculated using the numerical integral by the following relationship (Eq. (3)) [8]:

$$Q = \sum_{n=1}^{N} F(n) - [X(n) - X(n-1)] \qquad \text{Eq. (3)}$$

Where, F is applied load, X is rate of displacement, n number of points recorded by the tensile test software and Q is Failure Energy.

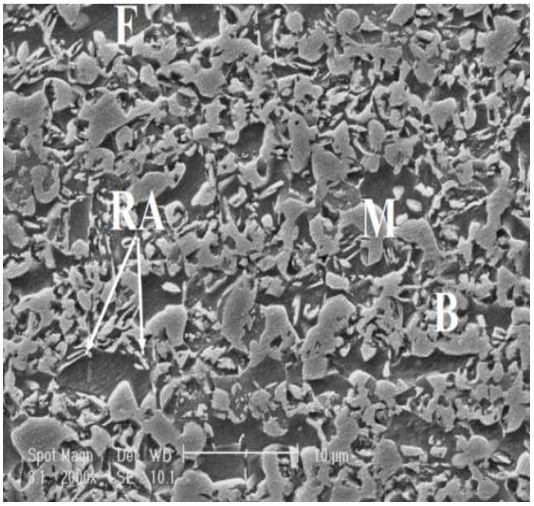

Fig. 2. Micrographs of the base materials, TRIP steel captured by SEM, (F: polygonal ferrite, M: martensite, B: bainite, RA: retained austenite, M/A: martensite/austenite island phase).

The area of weld cross-section in the HAZ and nugget area is presented in Fig. 3. for the samples presented in Table. 4. (these areas were calculated by Digimizer Software).

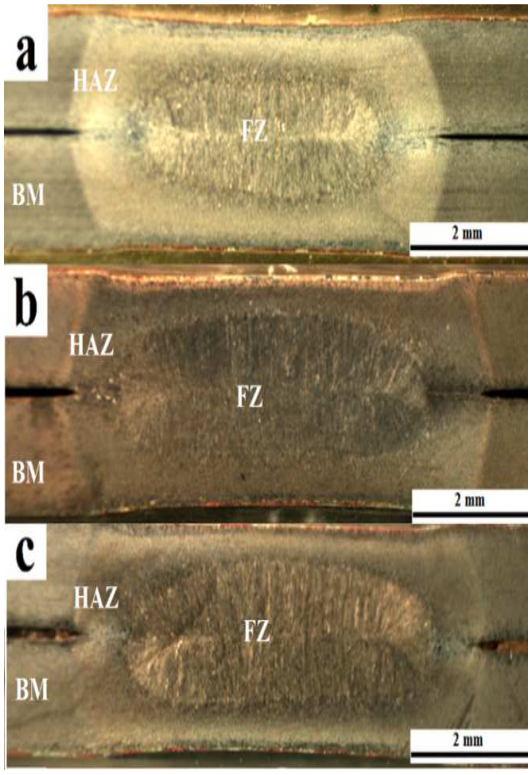

Fig. 3. Cross-section macrostructures of TRIP steel resistance spot welded samples with the following welding conditions: (a) Sample 1, (b) Sample 2 (c) Sample 3.

It can be said that more heat input and higher welding current lead to an increase in the length of the spot in between the sheets.

Fig. 4. shows the effect of welding parameters on the area of the nugget and HAZ for different samples. The macrostructure of the specimens presented in Fig. 5. shows the weld nugget boundary and HAZ clearly.

As shown in Fig. 5, less welding time in sample 1 produces smaller nugget than samples 2 and 3 with higher welding time.

FZ in samples 2 and 3 are roughly the same, but in sample 3, the HAZ size has increased at higher pressure, which is not desirable because the heat spread in the sheets is increased.

It can be said that forces of more than 3.5 do not lead to an increase in the size of the Nugget, and even prevents the growth of the Nugget, which is a consequence of the work of Zhou et al. [17].

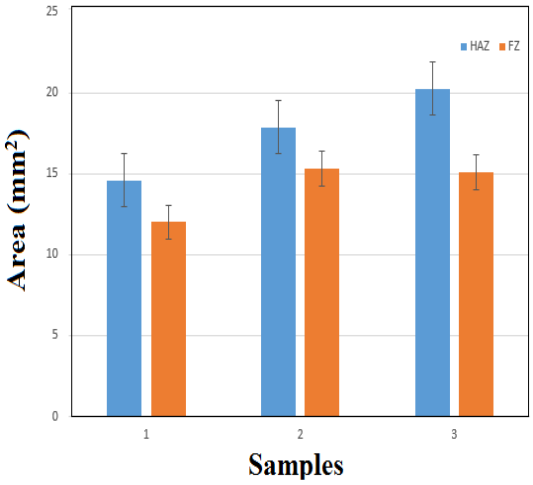

Fig. 4. The effect of welding parameters on the area of the nugget and HAZ on the different samples.

At first seen, the structure of the weld nugget contains the martensite phase due to the high cooling rate which is normally experienced during RSW.

Due to water cooled electrodes, the elongated columnar microstructure is observed in FZ as is evidenced by Fig. 6. Moreover, HAZ width of the sample 2 and 3(Fig. 5.b and Fig. 5.c) is larger than sample 1(Fig. 6.a) because of its higher heat input.

Fig. 6.c illustrates elongated columnar grains that meet each other at the weld centerline.

It was mentioned in a research by Pouranvari et al. [14] that the structure of HAZ transformed to predominantly martensite with small areas of ferrite, lath bainite, and retained austenite, depending on the ultimate temperature reached and cooling rate.

Transformation of austenite to bainite occurs at lower temperatures. Following that the remaining austenite transforms to martensite.

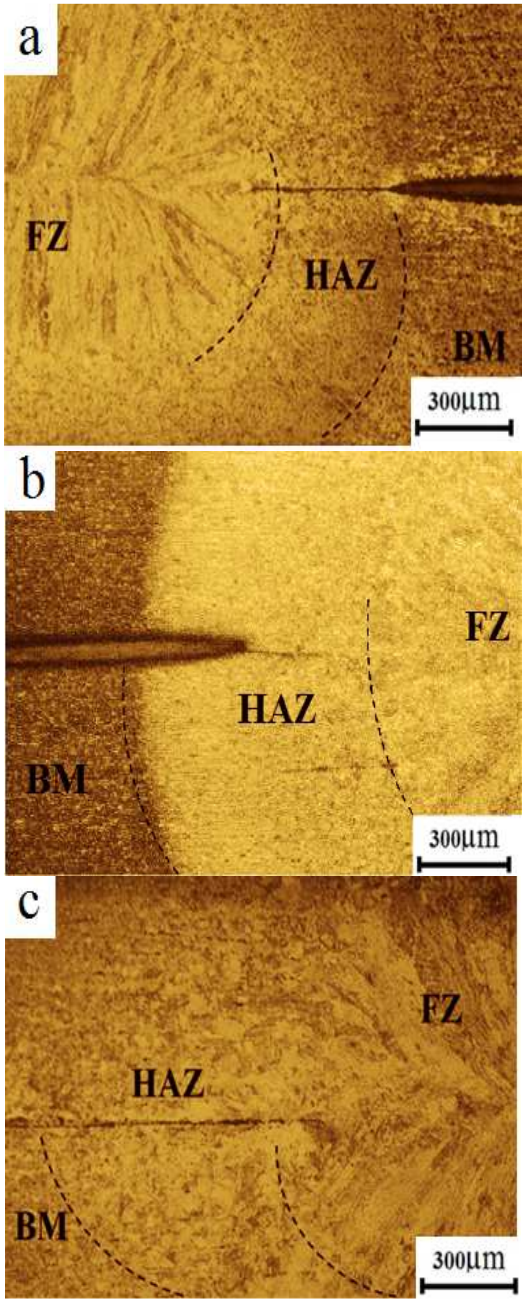

Fig. 5. The microstructure of the weld nugget, HAZ and BM, (a) Sample 1, (b) sample 2, (c) sample 3.

Figs. 6.a and Fig. 6.b show SEM micrographs of the center of the weld nugget and HAZ of the sample 2. It is noteworthy that the solidification structure (primary structure) is partially observed along with the solidification of the molten nugget.

In fact, it has been stated that solidification microstructures are developed in the interior and/or along the grain boundaries of the primary structure [5].

Directional columnar solidification from the fusion boundary towards the weld center line is seen in the weld nugget macrostructure (Fig. 3.).

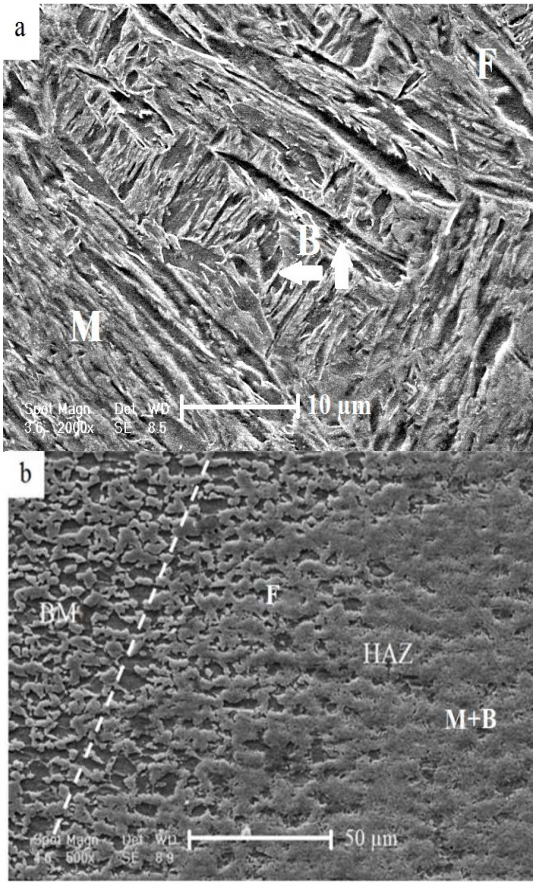

Fig. 6. SEM of (a) the center of the weld nugget and (b) HAZ, F ferrite, M martensite and B bainite.

The HAZ does not melt, but due to the temperature rise and then the rapid cooling, the microstructure will be different from the base metal.

As shown in Fig. 7., HAZ can be further divided into three distinct subzones.

These subzones consist of uppercritical HAZ (UCHAZ)[1], intercritical HAZ (ICHAZ)[2] and subcritical HAZ (SCHAZ)[3].

In the UCHAZ, where temperature exceeds Ac_3, the material is completely austenitized during welding thermal cycle (Fig. 7.a and Fig. 7.b).

In the ICHAZ, the temperature range is between Ac_1 and Ac_3 and the material is partially austenitized (Fig. 7.c).

In the lower or subcritical HAZ, the temperature is below Ac_1 and the martensite in this zone is tempered (Fig. 7.d).

Therefore, microstructure is not similar throughout the HAZ due to the temperature experienced.

[1] Uppercritical HAZ
[2] Intercritical HAZ
[3] Subcical HAZ

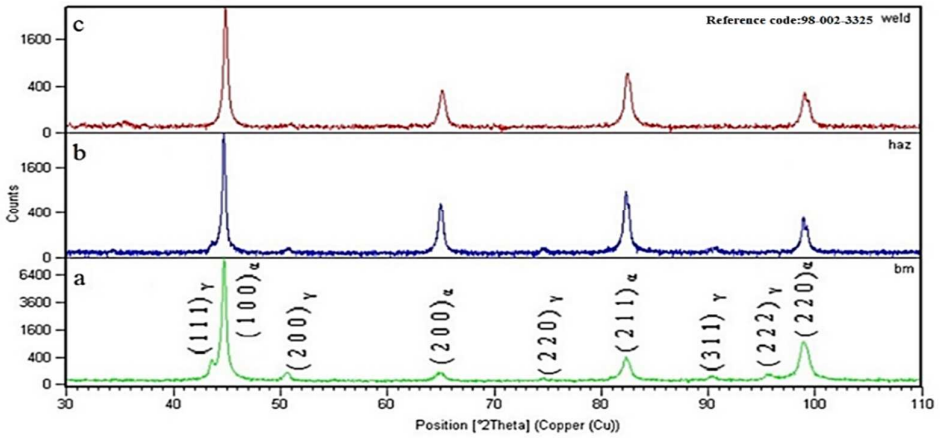

Fig. 8. XRD results for (a) BM, (b) HAZ and (c) FZ of TRIP steels spot weld (sample 2).

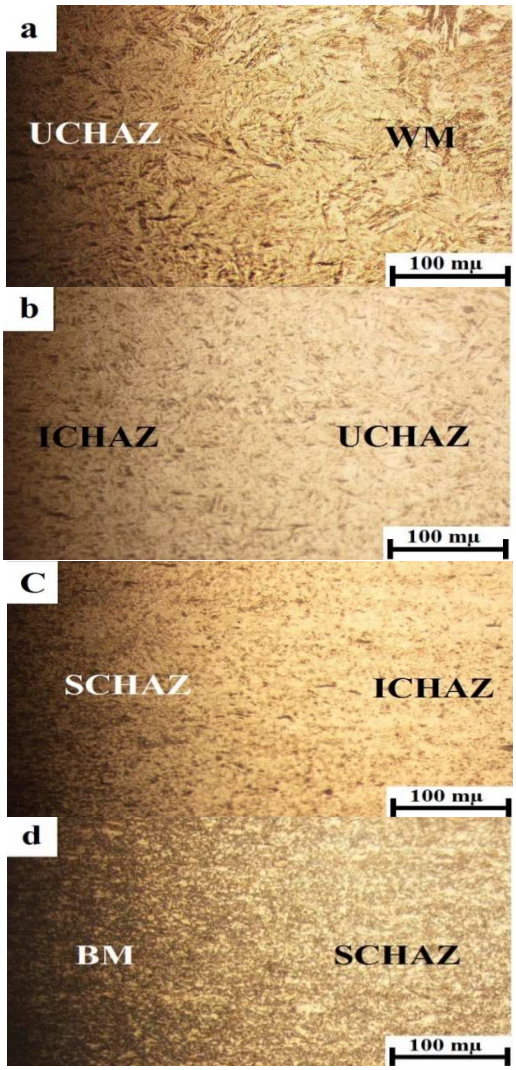

Fig. 7. Different subzones of HAZ microstructure (a, b) weld and upper critical HAZ, (b, c), intercritical HAZ, (d) subcritical critical HAZ and base metal for sample 2.

Fig. 8. shows the results obtained from XRD analysis on BM, HAZ and FZ of TRIP steel welds. BM analysis shows peaks of austenite and ferrite which is the main constituents observed using metallographic examinations. A reduction in the intensity of the austenite peaks and a slight increase in BCT martensite are observed within the HAZ.
This transition can be attributed to the mixture of austenite and martensite in the HAZ. No evidence of austenite peaks was recorded by XRD for the FZ, hence the predominately structure in this region is martensitic.

3.2. Strength and Fracture Relationships

The lap shear specimens, and test design are shown in Fig. 9.a. Tests were performed on these specimens to determine their load displacement curves. Fig. 9.b shows the typical load displacement curves for the TRIP steel spot welds; other results obtained from these curves are given in Table. 4.

Table. 4. Effect of welding parameters on the width of FZ and HAZ.

sample	Nugget Area (mm^2)	HAZ Area (mm^2)
1	12.01	14.59
2	15.30	17.85
3	15.09	20.24

The results in this study denoted that TRIP steel spot welds with nugget size more than $4\sqrt{t}$ nugget tend to fail by pullout failure mode, in addition the tensile shear strength of welds increased with an increase in the nugget diameter, base metal strength and thickness. Welding engineers have also adopted $4\sqrt{t}$ as the target nugget size for the mild steels. If weld nugget diameters were less than or equal to $2\sqrt{t}$, those welds would fail in the interfacial fracture mode in conventional steels which is unacceptable for the automotive industry and would be rejected.

In this study, all obtained welds were accepted by the above criterion [3]. pouanvari et al. [14] showed that pullout failure is accepted in the tensile shear tests. However, the weld nugget diameter criterion of $5\sqrt{t}$ can produce pullout fracture mode for the dual-phase steels.

To evaluate the spot weld mechanical behaviors, the tensile–shear (TS), cross tension (CT) and coach peel (CP) tests are widely used. Fig. 9.c shows the load–displacement curves with other data which can be derived from the tensile shear–test.

To explain the mechanical properties of the spot welds completely, one curve was prepared according to the loads-displacement curve that shows the maximum peak load (P_{max}) and elongation at maximum load (L_{max}). To determine the maximum flexibility value and impact absorption capacity, maximum absorbed energy, W_{max}, is defined. Table. 5. given the parameters derived from tensile–shear curve. As is observed, L_{max} and W_{max} of the sample 3 with electrode force of 4 kA and welding current of 10 kA are the highest values so this sample can have more flexibility and impact performance with regard to the nugget size and type of failure.

Table. 5. The derived data from tensile–shear curves.

Sample	W_{max}	P_{max}	L_{max}
1	2903.8	4910	1.9
2	5074.2	6855	1.2
3	13569.1	10050	2.7

Nugget Area (mm^2), of weldment was also given in Table. 4. Fig. 10. shows that the shear strength data are quite acceptable where the failure modes are described as partial plug.

To study the fracture and mode of development of the crack during application of shear forces in different stages, the sample stress was stopped in 3 different stages.

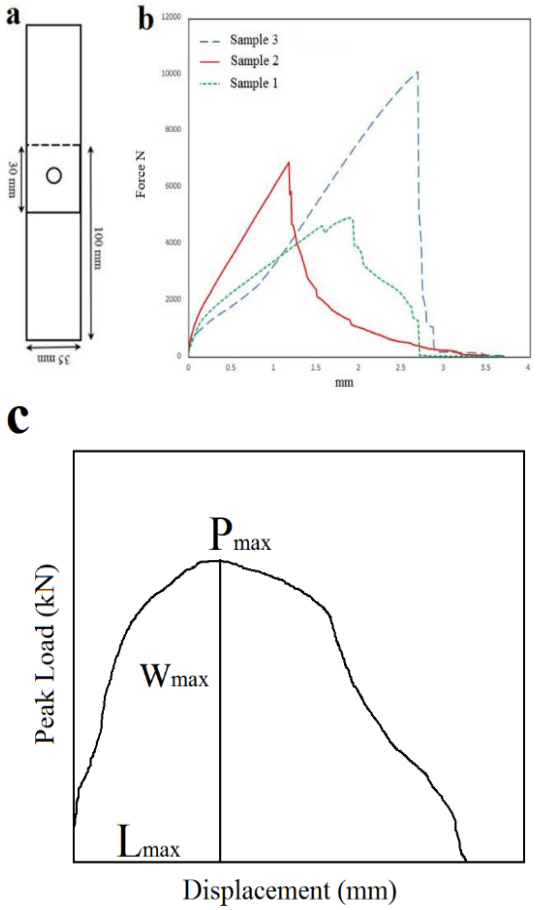

Fig. 9.(a) Lap shear coupon design, (b)Typical load versus displacement curves for TRIP steel welds and (c) load–displacement curve with the data which can be derived from the tensile-shear test.

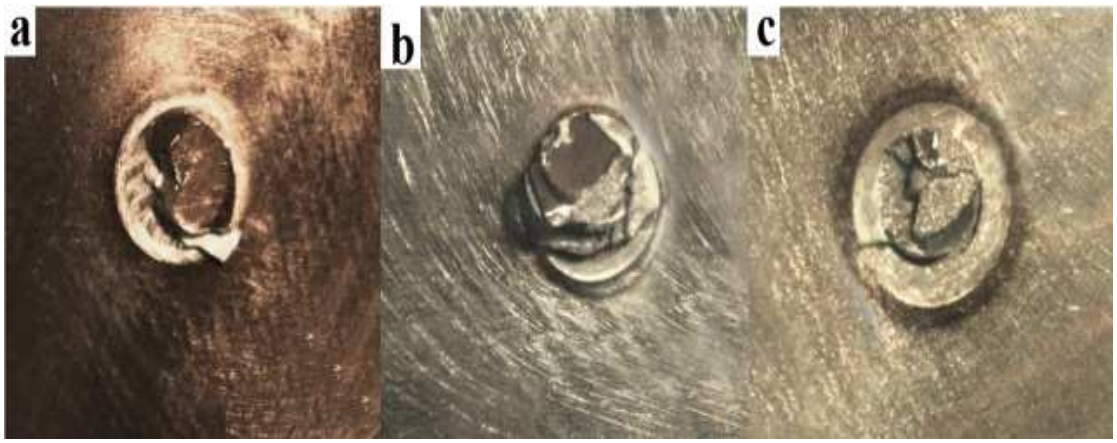

Fig. 10. Illustration of different failure modes (a, b) sample 1,2 interfacial fracture with partially button pull and partial thickness fracture, (c) sample 3, interfacial fracture with partial thickness fracture.

To investigate the microstructure of fracture, it is necessary to use SEM. As shown in Fig. 11.a fracture of the sample 1 is a mixture of interfacial fracture and weld pullout, for sample 2 approximately 30% interfacial fracture in the weld button is observed (see Fig. 11.b)[17]. In addition, partial interfacial fracture was also observed for sample 3 as can be seen in Fig. 11.c.

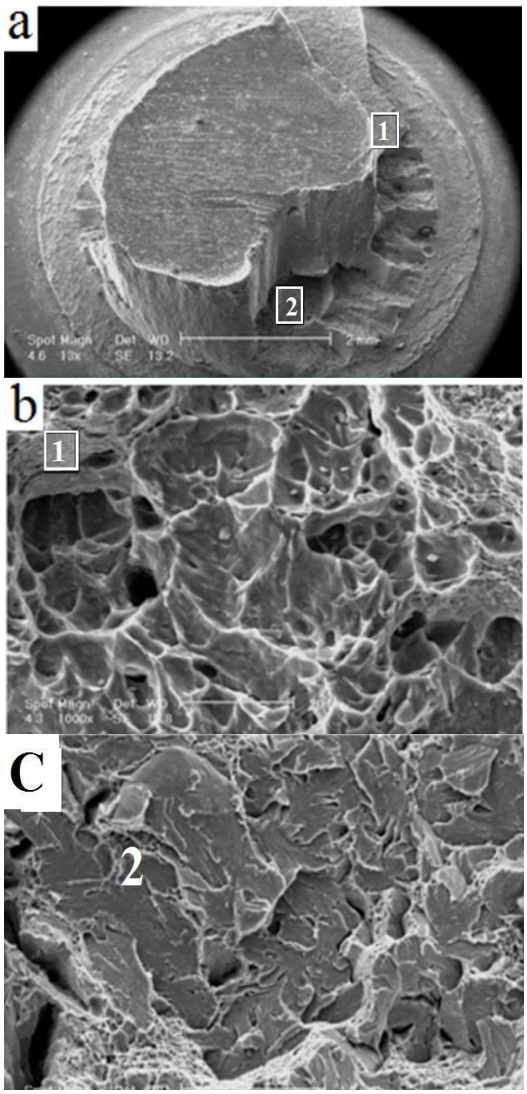

Fig. 11. a Microstructure of the fracture a) overall view a mixture of interfacial fracture and weld pullout, b) fracture with dimple-like ductile fracture characteristics, c) with cleavage fracture characteristics.

4. Conclusions

1. Austempering resulted in a microstructure composed of ferrite, bainite, retained austenite and a significant amount of martensite for TRIP steel.
As observed, microstructure of spot welds is complicated composed of martensite and bainite.

2. The results denoted that in lap-shear test, the crack nucleated at the tip of notch, which is a position of stress concentration.
The partial dome fractures could be characterized by the crack propagation along the border of the nugget close to UCHAZ.
3. Failure mode transition from interfacial to pullout failure mode was achieved for sample (10kA with 4kN). Partial interfacial failure (PIF) was removed after nugget size increased. Pullout failure mode is seen for the sample 2 (10kA with 3.5kN). The fractured surface in all samples showed dimple-like ductile fracture characteristics and transgranular fracture with cleavage facets, and the regions containing micro-void coalescence.

References

[1] S. Chatterjee: Transformations in TRIP-Assisted Steels: Microstructure and Properties, Darwin College: University of Cambridge at Cambridge, (2006).
[2] American Iron and Steel Institute, General Motors-AISI AAC Advanced High Strength Steel Repairability Study Phase II Final Report, (2015).
[3] Amirthalingam M. Microstructural Development during Welding of TRIP Steels. Delft: Delft University of Technology at Delft, (2010).
[4] L. Zhao, M. K. Wibowo, M. J. M. Hermans and S. M. C. Van Bohemen, J. Sietsma, J. Mater. Process. Technol., 209(2006), 5286.
[5] S. Brauser, L. A. Pepke, G. Weber and M. Rethmeier, Mater. Sci. Eng., A 527(2010), 7099.
[6] M. I. Khan, M. L. Kuntz, E. Biro and Y. Zhou, Mater. Trans., 49(2008), 1629.
[7] I. Hajiannia, M. Shamanian, M. Atapour, E. Ghassemali and N. Saeidi, Trans. Indian Inst. Met. 71(2018), 1363.
[8] Russo Spena P, De Maddis M, D'Antonio G, Lombardi, Metals, 6 (2016), 1.
[10] R. Ohashi, Weld World, 55(2011), 2.
[11] H. Gaul, S. Brauser, G. Weber and M. Rethmeier, Weld World, 55(2011), 99.
[12] G. Weber, S. Goklo, Weld World, 50(2006), 3.
[13] J. Pakkanen, R. Vallant, M. Kicin, Weld World, 60(2016), 3.
[14] M. Pouranvari, S. M. Mousavizadeh, Mat. Tech., 47(2013), 771.
[15] Z. Hou, S. Kimb, Y. Wang, C. Li and C. Chen, J. Mater. Process. Technol., 185(2007), 160.
[16] V. H. Hernandez Baltazar, S. K. Panda, M. L. Kuntz and Y. Zhou, Mater. Let., 64(2010), 207.
[17] K. Zhou, and CAI, J. Appl. Phys., 116(2014) 084902.